OPEN ACCESS Freely available online

Journal of Pollution Effects & Control

Research Article

# Rapid Detecting and Removing of Carcinogenic Hydrocarbons for Polluted Water Treatment Based Electrochemical Assay and Chemical $Fe_3O_4$ Nanoparticles Synthesis

**Rand Salah Khalifa[1*], Hisham Faiadh Mohammad[2,3], Makia Mohalhul Al-Hejuje[1]**

*[1]Department of Ecology, College of Science, University of Basrah, Basrah, Iraq; [2]Department of Biology, College of Science, University of Basrah, Basrah, Iraq; [3]Department of Pharmacy and Bioengineering, Keele University, keele, Iraq*

## ABSTRACT

Herein, the single strand ssDNA nanoreceptor was mixed with $Fe_3O_4$ nanoreceptor were fabricated chemically based a molecular recognition probe binding electroactive redox probe Methylene Blue (MB) to the surface of screen printed gold electrode was created and modified for rapid, highly sensitive and specific detection of hydrocarbons. For the electrochemical ssDNA based nanoreceptor assay of hydrocarbon detection and treatment, less than an 1 hour was needed in time. The total concentrations of aliphatic compounds ranged for the three stages before treatment (301.69-3512.41), (161.68-2281.62) and (112.79-1539.44), respectively, while after treatment, the concentrations for three stages became (0-1554.45), (0-1005.92) and (0-631.76), respectively, the treatment efficiency was in the three stages (56.1%-91.3%), (48.2%-73.9%) and (44.6%-76.5%) respectively. Moreover, the total concentrations of aromatic compounds before nanotreatment ranged for the three stages before treatment (56.26-881.94), (38.85-587.36) and (15.02-218.12) respectively, while After treatment, the concentrations in three stages became (0-459.5), (0-95.9425) and (0-80.195) respectively, the treatment efficiency was for the three stages (26.5% winter-66.67% autumn), (28.7%winter-66.7% autumn) and (9.08% winter-33.3% summer), respectively.

**Keywords:** Rapid detecting; Single-stranded DNA; Chemogenic; Carcinogenic hydrocarbons; Nanoparticles

## INTRODUCTION

A complex mixture of hydrocarbons, including crude oil and its refined by products, change in their properties depending on the quantity of carbon and hydrogen atoms in the molecule and how the atoms are arranged. Arrangements such as cyclic, branching or straight chains (aromatic compound with fused benzene rings). The crude oil and refinery references also include sulphur, nitrogen, oxygen and some trace components. The primary component of crude oil and petroleum derivatives, hydrocarbon molecules, are extremely poisonous to all living things, including humans, in higher concentrations. The harmful sulfur and nitrogen molecules found in trace levels in petroleum products can react with the primary pollutant to form secondary dangerous chemical [1]. The final disposal of produced water can contaminate surfaces, groundwater and soil if it is not properly treated. Therefore, in order for oil field produced water to be dumped into the ocean, re-injected into reservoirs or even used for irrigation, these components must be decreased or entirely removed using some form of treatment (chemical, physical, biological or a combination of two or more of these components [2]. Because of the groundbreaking developments in nanoscience and nanotechnology over the past 20 years, the scientific community is investigating this promising area of research, where it may be possible to use the special and advantages of new nanostructured materials to offer more long-lasting and effective solutions to the present water-related issues [3]. Water treatment is a major problem in underdeveloped nations because of poor management, erratic supply, contamination and a lack of chlorination [4]. Innovative approaches to water filtration have been made possible by nanotechnology [5]. Nanomaterials are typically 1 nm to 100 nm in size. They contain far less atoms due to their tiny size; this gives them significantly distinct characteristics from bulk

**Correspondence to:** Rand Salah Khalifa, Department of Ecology, College of Science, University of Basrah, Basrah, Iraq; E-mail: hisham.mohammed@uobasrah.edu.iq

**Received:** 28-Sep-2024, Manuscript No. JPE-24-34390; **Editor assigned:** 02-Sep-2024, PreQC No. jpe-24-34022 (PQ); **Reviewed:** 16-Oct-2024, QC No. JPE-24-34390; **Revised:** 10-Jun-2025, Manuscript No. JPE-24-34390 (R); **Published:** 17-Jun-2025, DOI: 10.35248/2375-4397.25.13.441

**Citation:** Khalifa RS, Mohammad HF, Al-Hejuje MM (2025) Rapid Detecting and Removing of Carcinogenic Hydrocarbons for Polluted Water Treatment Based Electrochemical Assay and Chemical $Fe_3O_4$ Nanoparticles Synthesis. J Pollut Eff Cont. 13:441.

materials. Due to their small size, nanomaterials have an extraordinarily high surface area to volume ratio, which results in more surface-dependent properties. Nanomaterials have been found to have advantageous physicochemical characteristics that make them effective adsorbents for a variety of water pollutants [6]. Using nanotechnology for water filtration depends on the stage of filtration that it has been applied to. Nanotechnology can be used to eliminate various germs, harmful substances including arsenic and mercury and sediments. Although there are hazards associated with nanomaterials because they have a high surface area to volume ratio and are very reactive, there are no known issues with human health or the environment related to water purification using nanotechnology [7]. The proposed sensing technique was effectively used to eliminate hydrocarbons from water samples. The developed electrochemical assay based nanoreceptor demonstrated high specificity for hydrocarbons. The study proved the efficiency of nanotechnology in removing petroleum hydrocarbons compared to the conventional treatment methods in the station. In addition, nanoparticles can be prepared in an easy chemical and biological way.

# MATERIALS AND METHODS

## The area of study

The plant has an overall oil treatment capacity of 200 kbopd over four new crude oil separation trains (50 kbopd each) and an overall water injection capacity of 450 kbwpd at 190 barg with 4 water injection pumps (3+1 spare) with a capacity of 150 kbpwd each. Produced water in order to meet water injection specifications, produced water treatment facilities was installed with total a capacity of 240 kbwpd (4 trains of 60 kbwpd each). Storage facilities include 3 stabilized oil flow tanks (working capacity of 75 kbbl each), an off-spec oil tank (15 kbbl). Two intermediate produced water tank (33 kbbl each), two water injection tanks (62 kbbl each), two fire water tanks, (86 kbbl each), furthermore, the plant is equipped with Integrated Control and Safety Systems (ICSS), which allows to monitor and control all the units from the central control building ensuring a safe and reliable operation of the plant (Figure 1).

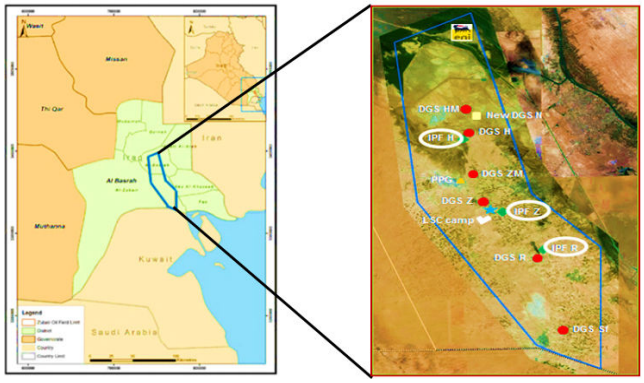


**Figure 1:** The area of study in Al-Zubair oil field.

## Fieldwork and measurements

Fieldwork and measurements were done seasonally from October 2021 to August 2022, in Hammar Mishrif station. Water turbidity (WTurb: NTU) was measured in the field using a turbidity meter. Water temperature (WT:°C), salinity (Sal: PSU) and electrical conductivity (EC: ms/cm) were measured *in situ* using the WTW cond 3310 set 1 and the WTW pH 3110 set 2 respectively. Prior to usage, the devices were calibrated.

## Water samples

Water samples as duplicate were collected from the Hammar Mishrif plant at three stages. Dark glass bottles were used to directly collect approximately 1 L at each stage (for petroleum hydrocarbon analysis, which preserved *in situ* with 25 ml chloroform).

## Chemo genic synthesis of $Fe_3O_4$ nanoparticles

In room temperature, aqueous solutions of the iron chlorides $FeCl_2$ and $FeCl_3$ (Figure 2A and B) were combined in a 1:2 molar ratio. Then 12.5 weight percent of an aqueous ammonia solution was progressively added [8]. The chemical process predicts that magnetite will result:

$$FeCl_2+2FeCl_3+8NH_4OH \rightarrow Fe_3O_4+8NH_4Cl+4H_2O.$$


**Figure 2:** Chemogenic method of $Fe_3O_4$ nanoparticles. **Note:** (A) Dropping ammonia solution to the chemical mixture, (B) $Fe_3O_4$ nanoparticles.

## Nano-drop (Dropsens) system

The AUTOLAB Dropsense electrochemical analysis system with gold printed electrodes (GPES 4.5 software package) was used to conduct the electrochemical measurements. Gold electrodes with screen printing were purchased from Dropsens-metrohm (www.metrohm.com). At a regulated temperature (25°C), the electrochemical experiments were performed. An electrochemical cell with screen printing that measures 3 by 1.5 cm is made up of a gold working electrode, a gold counter electrode and a silver pseudoreference electrode (Figure 3A and B).


**Figure 3:** Nano-drop (Dropsens) system. **Note:** (A) Dropsens potentiostat, (B) Screen printed gold electrodes

## DNA aptamer nanoreceptors preparation

Single stranded salmon testis DNA (ST ssDNA) were prepared in the lab *via* QIAGEN extraction kit see Cat. No. 69556 and Figure 4A and B. This protocol is designed for extraction and purification of total DNA from blood and animal tissues.

## Extraction and purification of ST ssDNA nanoreceptors

This protocol is designed for extraction and purification of total DNA from animal tissues. Important points before starting, if using the DNeasy blood and tissue kit for the first time, read "Important Notes" for fixed tissues, all centrifugation steps are carried out at room temperature (15°C-25°C) in a microcentrifuge. Vortexing should be performed by pulse-vortexing for 5-10 s. Optional: RNase A may be used to digest RNA during the procedure. RNase A is not provided in the DNeasy blood and tissue kit. Things to do before starting buffer ATL and buffer AL may form precipitates upon storage. If necessary, warm to 56°C until the precipitates have fully dissolved. Buffer AW1 and Buffer AW2 are supplied as concentrates. Before using for the first time, add the appropriate amount of ethanol (96%-100%) as indicated on the bottle to obtain a working solution. Preheat a thermomixer, shaking water bath or rocking platform to 56°C for use in step 2. If using frozen tissue, equilibrate the sample to room temperature (15°C-25°C). Avoid repeated thawing and freezing of samples, because this will lead to reduced DNA size. DNeasy Blood and Tissue Handbook 07/2020 31 procedure.

- Cut up to 25 mg tissue into small pieces and place in a 1.5 ml microcentrifuge tube. We strongly recommend cutting the tissue into small pieces to enable more efficient lysis. If desired, lysis time can be reduced by grinding the sample in liquid nitrogen before addition of buffer ATL and proteinase K. Alternatively, tissue samples can be effectively disrupted before proteinase K digestion using a rotor–stator homogenizer, such as the tissue ruptor II or a bead mill, such as the tissue lyser II. A supplementary protocol for simultaneous disruption of up to 48 tissue samples using the tissue lyser II can be obtained by contacting QIAGEN technical services.
- Add 20 µl proteinase K. Mix thoroughly by vortexing and incubate at 56°C until the tissue is completely lysed. Vortex occasionally during incubation to disperse the sample or place in a thermomixer, shaking water bath or on a rocking platform. Lysis time varies depending on the type of tissue processed. Lysis is usually complete in 1–3 h or. If it is more convenient, samples can be lysed overnight; this will not affect them adversely. After incubation the lysate may appear viscous, but should not be gelatinous as it may clog the DNeasy mini spin column. If the lysate appears very gelatinous. When working with chemicals, always wear a suitable lab coat, disposable gloves and protective goggles. For more information, consult the appropriate Safety Data Sheets (SDSs), available from the product supplier. Optional: If RNA-free genomic DNA is required, add 4 µl RNase A (100 mg/ml), mix by vortexing and incubate for 2 min at (15°C-25C°) before continuing with step 3.
- Vortex for 15 s. Add 200 µl Buffer AL to the sample and mix thoroughly by vortexing. Then add 200 µl ethanol (96%-100%) and mix again thoroughly by vortexing. It is essential that the sample, buffer AL and ethanol are mixed immediately and thoroughly by vortexing or pipetting to yield a homogeneous solution. Buffer AL and ethanol can be premixed and added together in one step to save time when processing multiple samples. A white precipitate may form on addition of buffer AL and ethanol. This precipitate does not interfere with the DNeasy procedure.
- Pipet the mixture from step 3 (including any precipitate) into the DNeasy mini spin column placed in a 2 ml collection tube. Centrifuge at ≥ 6000 × g (8000 rpm) for 1 min. Discard flow-through and collection tube.
- Place the DNeasy mini spin column in a new 2 ml collection tube, add 500 µl buffer AW1 and centrifuge for 1 min at 5000 × g (8000 rpm). Discard flow-through and collection tube. Flow-through contains Buffer AL or Buffer AW1 and is therefore not compatible with bleach.
- Place the DNeasy Mini spin column in a new 2 ml collection tube, add 500 µl Buffer AW2 and centrifuge for 3 min at 20,000 × g (14,000 rpm) to dry the DNeasy membrane. Discard flow-through and collection tube. It is important to dry the membrane of the DNeasy mini spin column, since residual ethanol may interfere with subsequent reactions. This centrifugation step ensures that no residual ethanol will be carried over during the following elution. Following the centrifugation step, remove the DNeasy mini spin column carefully so that the column does not come into contact with the flow-through, since this will result in carryover of ethanol. If carryover of ethanol occurs, empty the collection tube, then reuse it in another centrifugation for 1 min at 20,000 × g (14,000rpm).
- Place the DNeasy Mini spin column in a clean 1.5 ml or 2 ml microcentrifuge tube and pipet 200 µl Buffer AE directly onto the DNeasy membrane. Incubate at room temperature for 1 min and then centrifuge for 1 min at 5000 × g (8000 rpm) to elute. Elution with 100 µl increases the final DNA concentration in the eluate, but also decreases the overall DNA yield.
- Recommended: For maximum DNA yield, repeat elution once as described in step 7. This step leads to increased overall DNA yield. A new microcentrifuge tube can be used for the second elution step to prevent dilution of the first eluate. Alternatively, to combine the eluates, the microcentrifuge tube from step 7 can be reused for the second elution step. Note: Do not elute more than 200 µl into a 1.5 ml microcentrifuge tube because the DNeasy Mini spin column will come into contact with the eluate.


**Figure 4:** DNA nanoreceptors extraction, **Note:** (A) ST tissue and (B) weighted samples

# RESULTS AND DISCUSSION

## Extraction of ssDNA aptamer nanoreceptors

All genital papilla tissue of salmon fish (*Oncorhynchus salmoninae*) (L-1758) which contain DNA was successfully extracted. Gel electrophoresis was used to detect band after separation using PCR as mention in ssDNA preparation and shown in Figure 5.

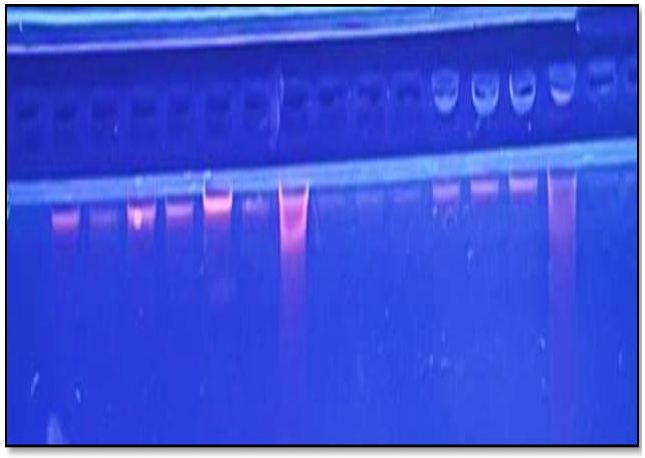

**Figure 5:** Gel electrophoresis for DNA band detection.

## $Fe_3O_4$ nanoparticles synthesis

The chemogenic synthesized nanoparticles of $Fe_3O_4$ were formed as shown in Figure 6.


**Figure 6:** Chemogenic method of $Fe_3O_4$ nanoparticles.

## $Fe_3O_4$ nanoparticles characterization

The SEM and TEM image of $Fe_3O_4$ nanoparticles was showed in Figures 7 and 8 respectively, in addition to the U.V, FTIR and XRD images that shown in Figures 9 and 10 respectively.

## Scanning Electron Microscopy (SEM)

The scanning electron microscope FEI-Nova SEM has been used in this research. In Figure 7, the spherical iron oxide grains with sizes of a few nanometers are clearly visible, indicating a successful synthesis of extremely small iron oxide nanostructures.

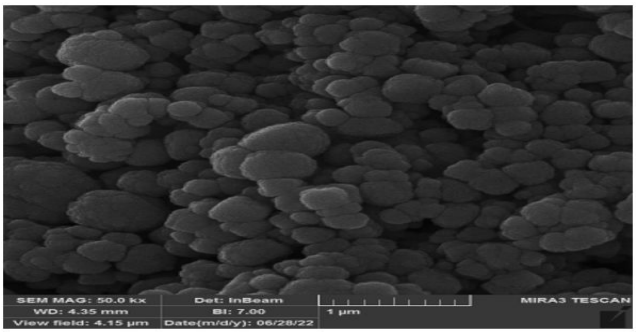


**Figure 7:** SEM image of $Fe_3O_4$ nanoparticles. The images clearly illustrated that the average size of the particles was found to be approximately 125 nm and spherical in shape.

## Transmission Electron Microscopy (TEM)

The images of iron oxide in TEM JEM-F200 model were displayed in Figure 8. The SEM and TEM data show that nanoparticles are roughly spherical and these results are consistent with one another.

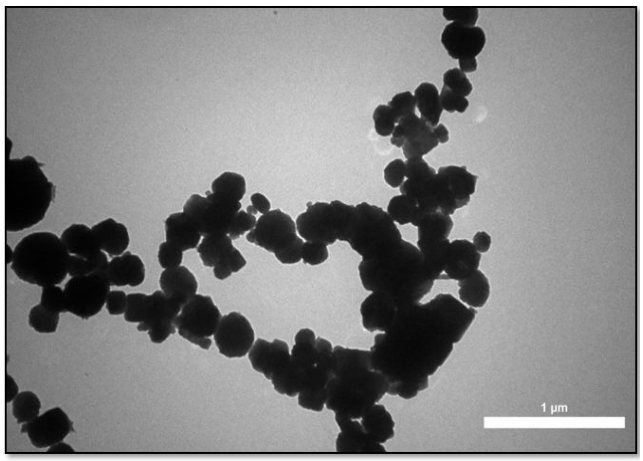


**Figure 8:** TEM image of $Fe_3O_4$ nanoparticles.

## Ultraviolet-visible spectroscopy

The SPECORD PLUS UV/Vis spectroscopic measurement 1200 nm was used in this study. prepared samples of bare, zinc, nickel and cobalt doped iron oxide nanoparticles have all undergone UV-vis spectral analysis. The UV-visible absorption spectra of iron oxide nanoparticles are displayed in Figure 7. The spectra show an iron oxide typical absorption peak at a wavelength of 190-200 nm, which is almost close to the iron oxide nanoparticle characteristic wavelength (Figure 9).

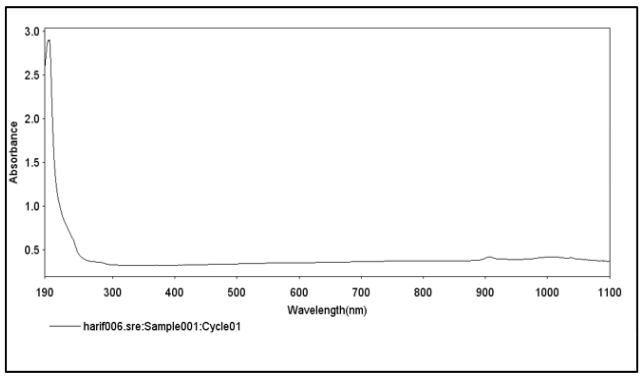


**Figure 9:** U.V spectra of magnetic iron oxide nanoparticles.

## Fourier Transform Infrared Spectroscopy (FTIR)

The FTIR 7800A fourier transform infrared spectrometer spectra are captured between 350 and 500 $cm^{-1}$. Iron oxide nanoparticles' FTIR spectra are displayed in Figure 10.

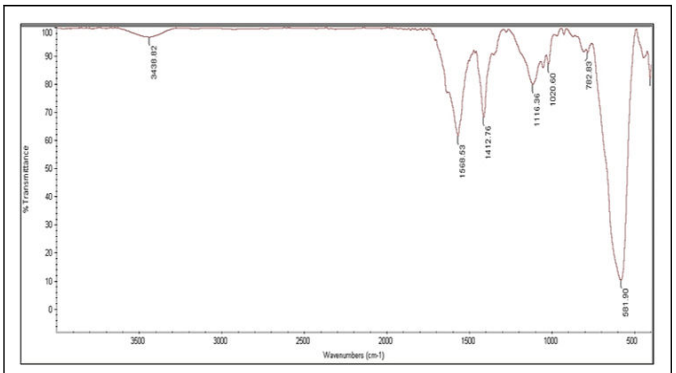


**Figure 10:** FTIR spectra of magnetic iron oxide nanoparticles.

## X-ray diffraction

By using DW-XRD-Y3000 Model X-ray diffraction instrument XRD analysis, the crystal structure and phase analysis of magnetite nanoparticles were investigated. The synthetic magnetic nanoparticles' powder XRD pattern closely resembled that of crystalline magnetite $Fe_3O_4$ (Figure 11).

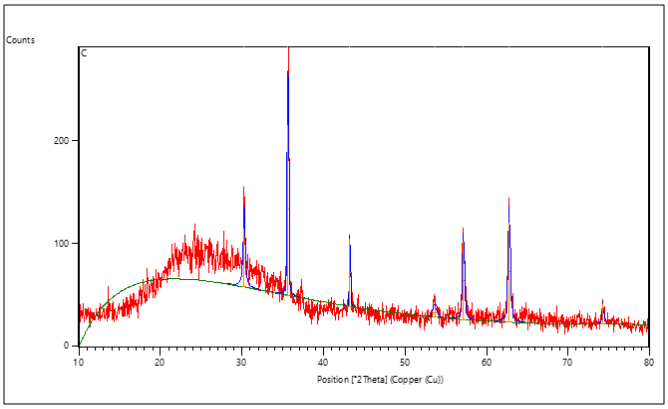


**Figure 11:** The XRD pattern of the synthesized $Fe_3O_4$ nanoparticles presented 6 intense peaks in the whole spectrum of 2θ values ranging from 20 to 80.

## Dropsense potentio stat electrochemical measurements

Typical Cyclic Voltammogram (CVs) recorded on modified screen-printed gold electrodes with immobilized ssDND in PBB solution with hydrocarbons in real polluted water are shown Figure 12. The anti-hydrocarbons ssDNA Figure 12 shows that a probe with a methylene blue redox group displayed well-resolved anodic and cathodic current peaks at about +0.2 V and -0.2 V, respectively, which corresponded to methylene blue and there is no oxidation and reduction peaks (B). The presence of hydrocarbons in the water samples is clearly correlated with the amplitudes of those two peaks; the current increases when the ss DNA probe binds the contents of the hydrocarbons, as was explained in the in previous section. The current peak was registered at potentials of about ± 0.2 V. Again, a correlation between the values of current and hydrocarbons binding is apparent and proves the immobilization and removal method concept in Figure 12. Control measurements were made using three-electrode assemblies lacking the target analyte, total

petroleum hydrocarbons, in order to eliminate the impact of hydrocarbons on the conductivity of HBB solutions. Figure 12 displays these data, which showed that there were redox group-related current peaks present and rather a monotonous increase in anodic and cathodic currents above their respective potentials of roughly 0.4 V after binding. The most important thing to note is that, in comparison to those shown on Figure 12, that the current increase at voltages of 0.2 V was very negligible. Real water samples from various local natural resources were examined using CVs measurements on screen-printed electrodes with anti-hydrocarbon ssDNA probe modified $Fe_3O_4$ nanoparticles immobilized. A novel and new electrochemical method for the detection of TPH using ssDNA sequences which modified based on $Fe_3O_4$ nanoparticles was developed. The immobilization procedures of screen-printed gold electrodes with single-stranded DNA was occur depends on the 5'-end of negatively charge then covalently bound to the surface of (screen-printed gold electrodes) and act like probe for the direct detection of total petroleum hydrocarbons in a real polluted water as illustrated in Figure 12.

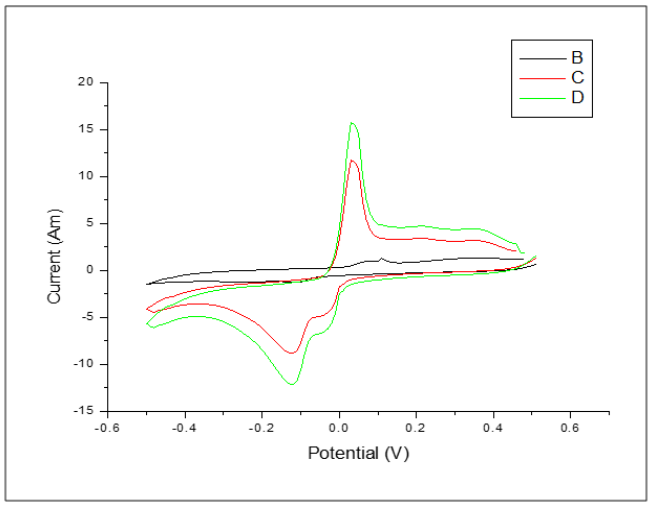


**Figure 12:** Dropsense potentio stat electrochemical measurements. **Note:** (A) The cyclic voltammogram result of ssDNA probe before binding, (B) ssDNA probe after binding with TPH and (C) after mixed ssDNA with FeNPs and total petroleum hydrocarbon binding.

## CONCLUSION

The encouraging results which obtained and the efficiency of $Fe_3O_4$ nanoparticles in the presence of aptamer that locally prepared from salmon is high compared to the conventional treatment at the studied stages also there are compounds that have been treated 100% and other compounds that have been treated little, may be due to the size of the manufactured aptamer that was not compatible with these compounds. The PAHs compound seasonal values in water at first stage before nanotreatment showed that the lowest value for B(K)fluoranthene in autumn and highest value for Anthracene in summer and after nanotreatment the lowest value for Bss(K)fluoranthene in spring and highest value for Anthracene in summer. In second and third stages the seasonal variations before nanotreatment were the lowest value for B(K)fluoranthene in winter and the highest value for anthracene in summer. While after nanotratment the lowest value for B(K)fluoranthene in winter and the highest value for IND(1,2,3)pyrene in spring. The seasonal variations in total aromatic hydrocarbons before nanotreatment were the lowest value in third stage in winter and the highest value in first stage in summer and after nanotreatment the values still low in third stage in winter and high in first stage in summer but the compounds concentrations decreased. Significant differences ($P<0.05$) were found among stages and seasons. The removal efficiency of aromatic compounds was low in third stage and high in second stage. Seasonally the removal efficiency was low in winter and high in autumn.

## REFERENCES

1. Bryan G, Kelly P, Chesters H, Franklin J, Griffiths H, Langton L, et al. Access to and experience of education for children and adolescents with cancer: A scoping review protocol. System Rev. 2021;10(1):167.
2. Tehrani TH, Haghighi M, Bazmamoun H. Effects of stress on mothers of hospitalized children in a hospital in Iran. Iran J Child Neurol. 2012;6(4):39-45.
3. Hagglof B. Psychological reaction by children of various ages to hospital care and invasive procedures. Acta Paediatr Suppl. 1999;88(431):72-78.
4. Rawat N, Kumar P. Interventions for improving indoor and outdoor air quality in and around schools. Sci Total Environ. 2023;858(Pt 2): 159813.
5. Kumar P, Rawat N, Tiwari A. Micro-characteristics of a naturally ventilated classroom air quality under varying air purifier placements. Environ Res. 2023;217:114849.
6. Tomson M, Kumar P, Barwise Y, Perez P, Forehead H, French K, et al. Green infrastructure for air quality improvement in street canyons. Environ Int. 2021;146:106288.
7. Lucas de Oliveira EA, Favaro A, Raimundo-Costa W, Anhê AC, Ferreira DC, Blanes-Vidal V, et al. Influence of urban forest on traffic air pollution and children respiratory health. Environ Monit Assess. 2020;192(3):175.
8. Zeger SL, Thomas D, Dominici F, Samet JM, Schwartz J, Dockery D, et al. Exposure measurement error in time-series studies of air pollution: Concepts and consequences. Environ Health Perspect. 2000;108(5):419-426.